Journal of
Biomaterials and Tissue Engineering
Vol. 8, 1535–1542, 2018

RESEARCH ARTICLE

Stress Effect of Screw Insertion Angle for Base Plate Fixation on Humeral Spacer in Reverse Shoulder Arthroplasty

H. Çağdaş Basat[1] and Levent Kirkayak[2,*]

[1] *Ahi Evran University Faculty of Medicine Orthopedics and Traumatology Department, Kirsehir, 40200, Turkey*
[2] *Istanbul Technical University, Faculty of Mechanical Engineering, Istanbul, 34437, Turkey*

There have been numerous methods used for improving glenoid base plate stability in reverse shoulder arthroplasty. In this regard, screw insertion angle is the most significant parameter. Our claim is that screw insertion angle provokes changes in contact stress distribution on humeral spacer. We analyzed effect of 20 different models on humeral spacer with finite element analysis. This was comprised of 5 different screw angles, 4 different abduction positions of shoulder and five intact muscles (deltoid, teres major, infraspinatus, teres minor, subscapularis). The screw insertion angle affected stress distribution of humeral spacer and became more significant as the shoulder abduction reached 90 degrees where the maximum moment to the shoulder arm was applied. In addition, it is shown that screw insertion angle is not only an important parameter for the stress distribution but also the magnitude of the contact stress on humeral spacer due to the changes of direction of the transmitted load during the abduction. Contact stresses on quadrants of the humeral spacer could be influenced by changing screw insertion angle and shoulder abduction angle. Also, a screw insertion angle placement at 17 degrees provided the optimal stress distribution on the humeral spacer at all abduction positions of shoulder.

Keywords: Screw Insertion Angle, Reverse Shoulder Arthroplasty, Contact Stress, Humeral Spacer, Glenoid Baseplate, Finite Element Method.

1. INTRODUCTION

Reverse shoulder arthroplasty (RSA) has been used frequently for shoulder arthritis resulting from cuff tear arthropathy in elderly patients.[1–6] However, nowadays, RSA is also implemented for proximal humeral fractures and salvage procedure for the failed shoulder arthroplasty. Although there have been many improvements in implant technology and surgical technique for RSA, complication rates of RSA have reached up to 50% and are mostly due to glenoid component loosening.[2,7–10]

It is widely accepted that loosening of the glenoid component usually arises from particles resulting from polyethylene wear inducing osteolysis which leads to the component loosening.[2,10–13] Initial fixation of the component and stability should be achieved ideally to prevent the formation of polyethylene wear particles.[4,14,15] Furthermore, in RSA, component position, such as glenoid diameter, inferior tilt, inferior overhang, medialization of the center of rotation, reducing the neck-shaft angle and cup depth, are crucial for stability while the force couple of the shoulder joint also contributes to maintaining stability.[2,16,17] The impairment of the force couple due to the deficiency of rotator cuff muscles paves the way for increasing the shearing forces between the glenoid baseplate and bone, leading to base plate failure. This impairment also increases contact stress and stress concentration between the humeral spacer and glenosphere.[18,19] This has been the most challenging issue to solve and all the aforementioned parameters have to be optimized. In particular, with an increase in rotator cuff deficiency various scenarios could unfold that require complex biomechanical solutions. One of the challenges consists of determining the optimal screw insertion angle (SIA) for fixing the glenoid base plate to the bone. Hopkins et al.[20] showed that SIA is more significant than screw length and diameter. They observed that if the SIA is increased, stability between baseplate and bone can be improved. Yang et al.[17] emphasized the importance of the SIA to provide glenoid base plate stability in their study. They showed that screw insertion in a divergent pattern has less relative motion than parallel or convergent patterns between the baseplate and bone. A number of researchers have

*Author to whom correspondence should be addressed.

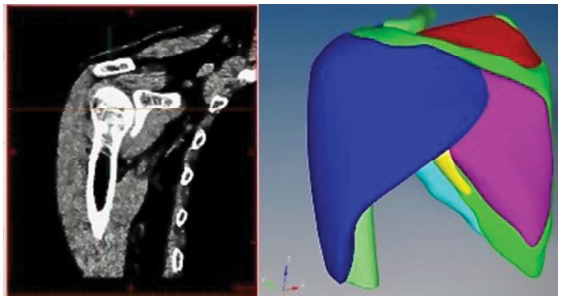

Fig. 1. Volume segmentation from CT scan and generated 3D model of left shoulder.

RESEARCH ARTICLE

reported about the influence of screw length, diameter and insertion angle on the shearing forces between bone and glenoid base plate, however they have only focused on early loosening of the glenoid component.[5, 7, 10, 14, 17, 20, 21] In our opinion, screw insertion angles may effect stress distribution on the humeral spacer via muscles due to the change of the load path across the glenoid bone-baseplate interface.

Up to now, no biomechanical study has examined the effect of screw insertion angles during the fixation of base plate to the glenoid and the stress generated upon the contact of the humeral spacer. The major objective of this study was to investigate relationship between the SIA and the contact stress distribution on the humeral spacer. For this purpose, we employed the three-dimensional finite element models that represented parts of the shoulder glenohumeral joint. In total, 20 different finite element models were generated with the combination of 5 different screw insertion angles and 4 different abduction positions of the shoulder.

2. MATERIALS AND METHODS

In order to gain significant insight into the aforementioned problem, the following techniques were employed: image analysis (volume segmentation) and finite element (FE) analysis, which were designed on the basis of the volume segmentation of the human shoulder.

2.1. Model Creation

In order to create 3-D model, first the image analysis was performed based on the left shoulder of a 40-year-old male subject without any shoulder pathology in terms of size and shape according to a computed tomography scan (CT). Using an image edition program, the segmentation of the different structures of the shoulder was performed, and the 1 mm thick volume rendering was implemented. After segmentation, the volume which was generated was delimited by a 2D triangular mesh. This mesh was exported to a pre-processor software which was used to create the 3D solid mesh (tetrahedral elements) directly from the triangular mesh (Fig. 1).

In order to analyze the effective parameters of the baseplate fixation methods, a three-dimensional model of the reversed shoulder prosthesis was also generated.

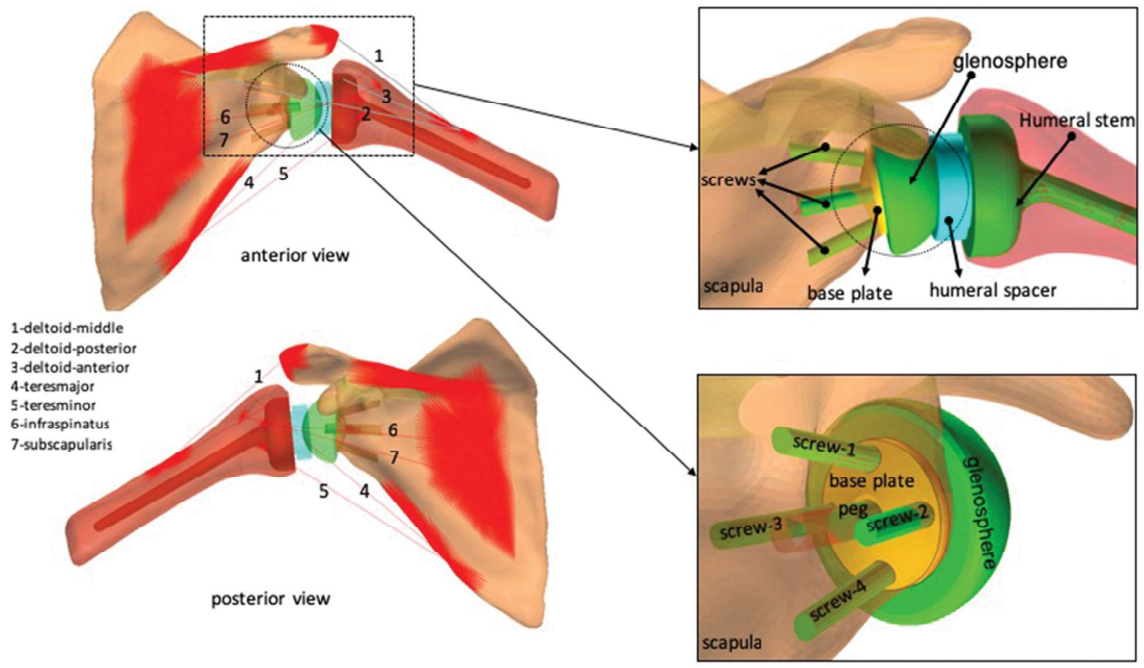

Fig. 2. The FE model of the reverse shoulder implant system.

Table I. The detail of finite element model.

Part	Material	Element information [number/type]	Young's modulus [GPa]	Poisson's ratio
Humerus cortical[26]	Bone	7139 /2D triangular, STRI65	20.7	0.3
Humerus cancellous[26]	Bone	40473/3D Tetrahedral, C3D10M	14.8	0.24
Scapula cortical[26]	Bone	21984/ 2D triangular, STRI65	20.7	0.3
Scapula cancellous[26]	Bone	76653/3D Tetrahedral, C3D10M	14.8	0.24
Plastic-spacer[33]	UHMWPE (Arcom)	26610/3D Tetrahedral, C3D10M	0.83	0.4
Glenoid[25]	CoNiCrMo	59187/ Tetrahedral, C3D10M	232	0.3
Implant[25]	CoNiCrMo	12842/3D Tetrahedral, C3D10M	232	0.3
Baseplate[24]	Ti6A14V	6980/3D Tetrahedral, C3D10M	115	0.33

Note: Numbers in the part column represent the reference which the related data is taken from.

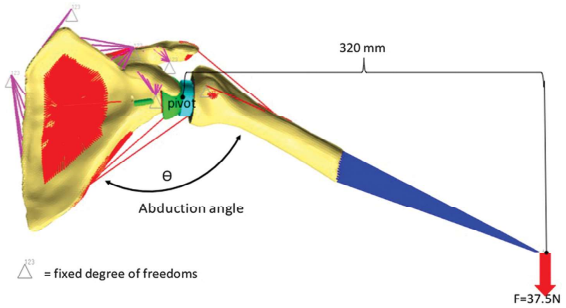

Fig. 4. The detailed FE models with abduction positions of the arm.

2.2. Finite Element Analysis

After the image analysis, a detailed geometrical 3-D FE model of the human shoulder was developed. The FE model consisted of following components: humerus and scapula bones and components of the Delta Xtend Reverse Shoulder System (Depuy, Warsaw, USA) (humeral spacer, glenosphere, baseplate, humeral stem and screws). The reverse shoulder implant system was placed into the bones according to the surgical technique of the manufacturer in a simulating computer environment. The humeroscapular rhythm was also considered and assessed at a 2:1 ratio.[4]

To decrease the computational effort, the human deltoid and other rotator cuff muscles (except for supraspinatus

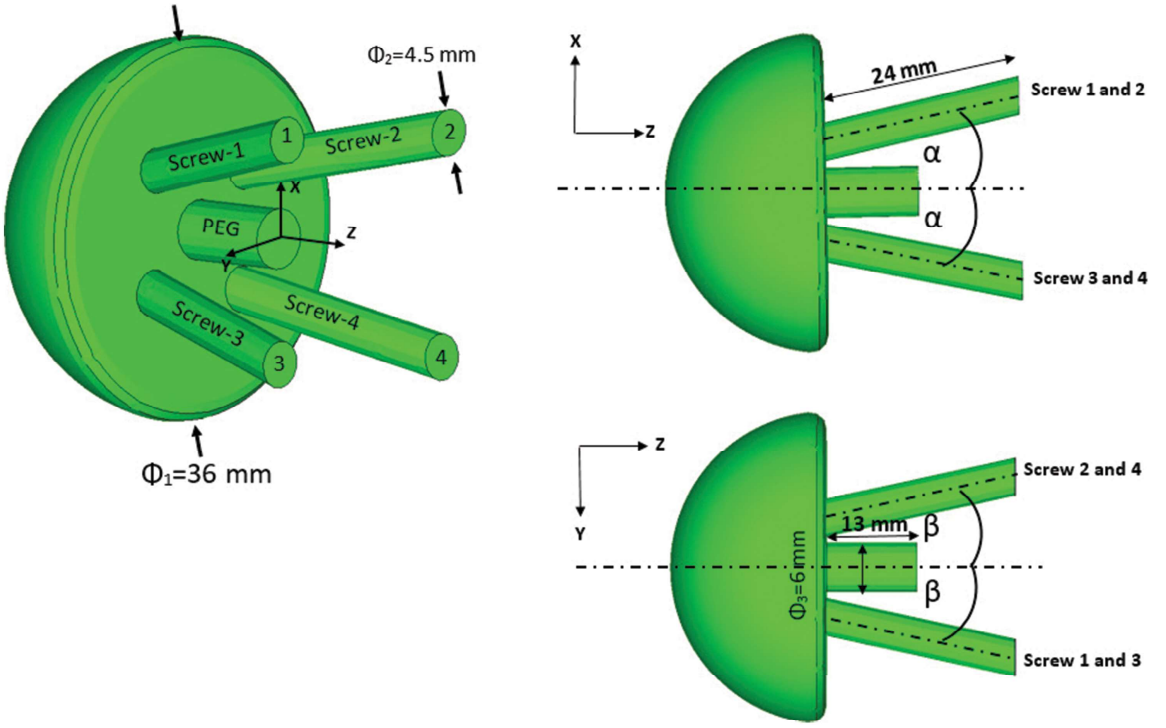

Fig. 3. Variation of screw insertion angle (α and β), (0, 10, 17, 25 and 34 degrees).

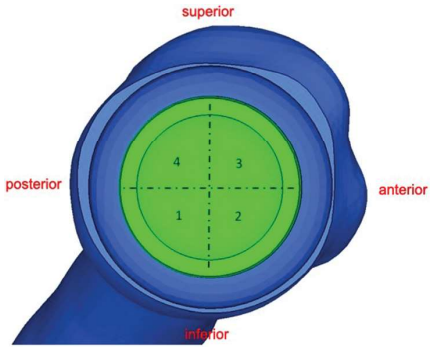

Fig. 5. Divided quadrants, according to mid-point of the tuberculum minus.

muscles) were represented by seven 1-dimensional (1D) non-linear spring elements (Fig. 2) and related stiffness values were obtained from literature.[22] Other soft tissues of the shoulder were not taken into account such as ligaments, joints and cartilage (Fig. 2).

The interfaces between bone and components of the implant were modeled as a consistent mesh. All components were modeled as isotropic, linear elastic materials with properties selected from literature (Table I).[23–26] The structure was meshed with different types of 3D tetrahedral elements with 10 node (C3D10M) except cortical parts of humerus and scapula. Those cortical parts were modeled with 6 node triangular shell elements (STRI65). Young's modulus and Poisson's ratio were assigned to each component. The element details and material information are given in Table I.[23–26]

Contacts between adjacent components such as glenosphere-humeral spacer, screws-scapula, implant-humeral spacer, baseplate-glenoid etc. were also considered in the model. These contacts were modeled as an element-based surface to surface type contact. The Coulomb friction was used for the tangential contact law and the friction coefficient (μ) was set to 0.001.[27]

In order to investigate the effects of the SIA (α) of the baseplate, 20 different finite element models were generated. These models include the combination of 5 different SIA (α) (0, 10, 17, 25 and 34 degrees, Fig. 3) and 4 different abduction positions of the arm (θ) (0, 30, 60 and 90 degrees, Fig. 4). Here in this study, the SIA(α) in X–Z plane was taken into account. The other insertion angle (β) in Y–Z plane was taken equal to the (α) due to the simplification (Fig. 3). The line crossing the mid-point of the tuberculum minus was used to divide the humeral spacer into superior and inferior parts. Also each hemisphere was divided into two parts. These quadrants were named by using counterclockwise direction with arabic numbers. The aim of this partitioning was to facilitate of analyses of the results (Fig. 5).

2.3. Boundary Conditions

Boundary conditions were imposed on several locations of the scapula. Acromion, corocoid process, medial and superior border of the scapula were fixed by employing spring elements (SPRINGA, $k = 100$ N/mm).[27] A net normal vertical force of 37.5 N was applied as an arm weight on a point that is 320 mm away from the humeral head based on the study of Terrier et al.[28] The model used for the FE Analysis was depicted in Figure 4.

3. RESULTS

In this section, finite element analysis results of the humeral spacer under static loading are presented. As stated before, 5 different screw insertion angles and 4 different abduction positions of shoulder were taken into account in order to obtain the effects of SIAs on the humeral spacer in reverse shoulder arthroplasty.

The compression of glenosphere on the humeral spacer generates contact stress. Therefore, the contact stress distribution on the humeral spacer was taken as a main characteristic parameter in this study. To do that, contact stresses for each quadrant of the humeral spacer were obtained by computer simulations and the average contact stresses were evaluated by using all elements in the corresponding quadrant. Then, the maximum and minimum of averaged contact stresses were determined accordingly. All stress results were presented through the Von Mises' equivalent stress fields.

According to these results which were given in Table II, the maximum average contact stress occurred on quadrant 3 while the shoulder abduction angle was 90 degrees and the SIA was 34 degrees. The minimum average contact stress was on quadrant 1 while the shoulder abduction angle was 0 degrees and the SIA was 34 degrees.

Table II. In 4 quadrants, changing contact pressure while changing screw insertion angle and shoulder abduction angle.

sia (°)	0	0	0	0	10	10	10	10	17	17	17	17	25	25	25	25	34	34	34	34
saa (°)	0	30	60	90	0	30	60	90	0	30	60	90	0	30	60	90	0	30	60	90
q1 (MPa)	0.80	4.26	5.52	5.35	0.80	4.19	5.52	4.81	0.81	4.28	5.20	5.04	0.80	4.19	5.52	4.75	0.78	4.24	4.85	3.95
q2 (MPa)	1.37	1.93	3.73	5.05	1.35	1.93	3.76	4.10	1.36	1.92	4.24	3.65	1.36	1.94	3.75	5.13	1.37	1.87	4.20	5.17
q3 (MPa)	0.89	3.01	4.47	5.74	0.90	3.01	4.46	4.91	0.87	2.98	4.34	4.82	0.89	3.01	4.47	6.12	0.88	2.99	4.37	6.75
q4 (MPa)	1.06	2.58	3.45	4.36	1.05	2.58	3.47	3.60	1.09	2.61	3.22	3.36	1.06	2.58	3.45	4.88	1.05	2.58	3.28	5.76

Note: Sia: Screw insertion angle, saa: Shoulder abduction angle, q: Quadrant.

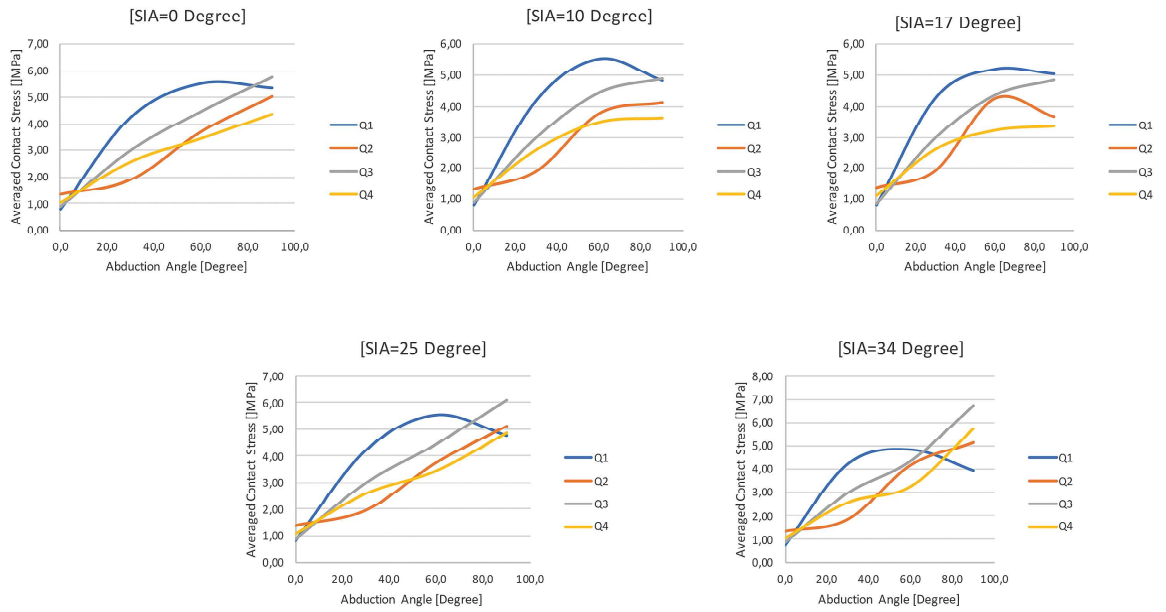

Fig. 6. Variation of stress distribution versus abduction angle.

It was also apparent from Table II that the average contact stress of quadrant 1 showed a nonlinear behavior during shoulder abduction and reached its maximum value in all 5 variations of SIA cases when the shoulder abduction was 60 degrees. After 60 degrees of abduction, the average contact stresses of the quadrant were decreased as the shoulder abduction angle reached 90 degrees.

In addition, as the SIA was fixed at 0, 10, 25 and 34 degrees, there was a positive relationship between average contact stress on quadrants 2, 3 and 4 and shoulder abduction angle. They were increased as long as the shoulder abduction was increased (Fig. 6).

Interestingly, as the SIA was fixed at 17 degrees (Fig. 6), the positive relationship between average contact stress

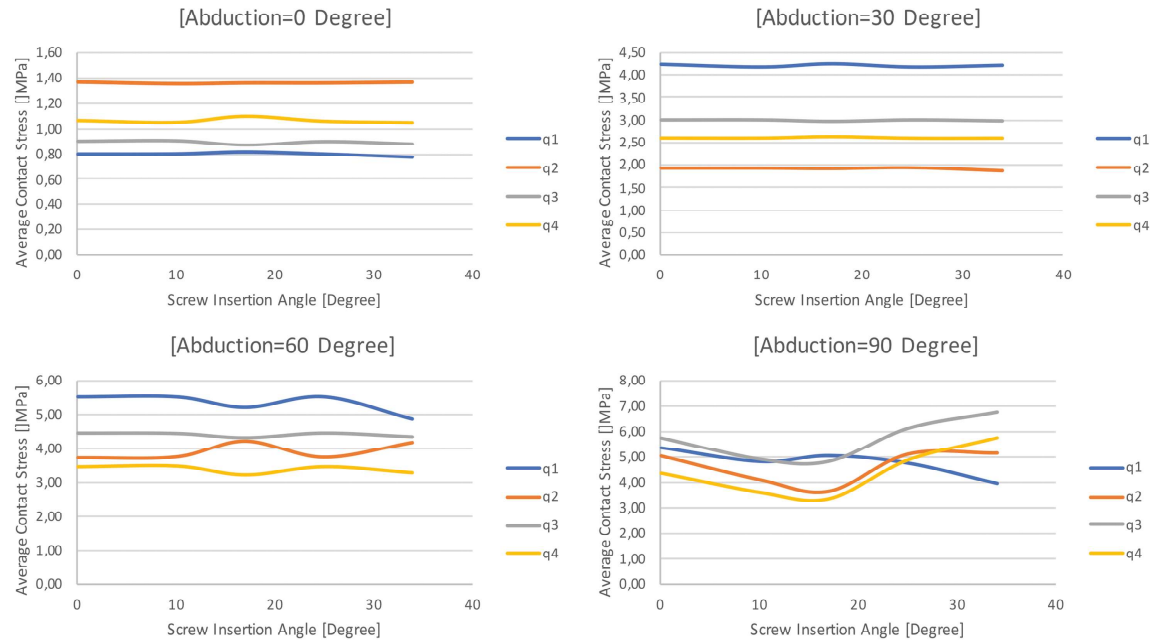

Fig. 7. Contact stress versus screw insertion angle.

RESEARCH ARTICLE

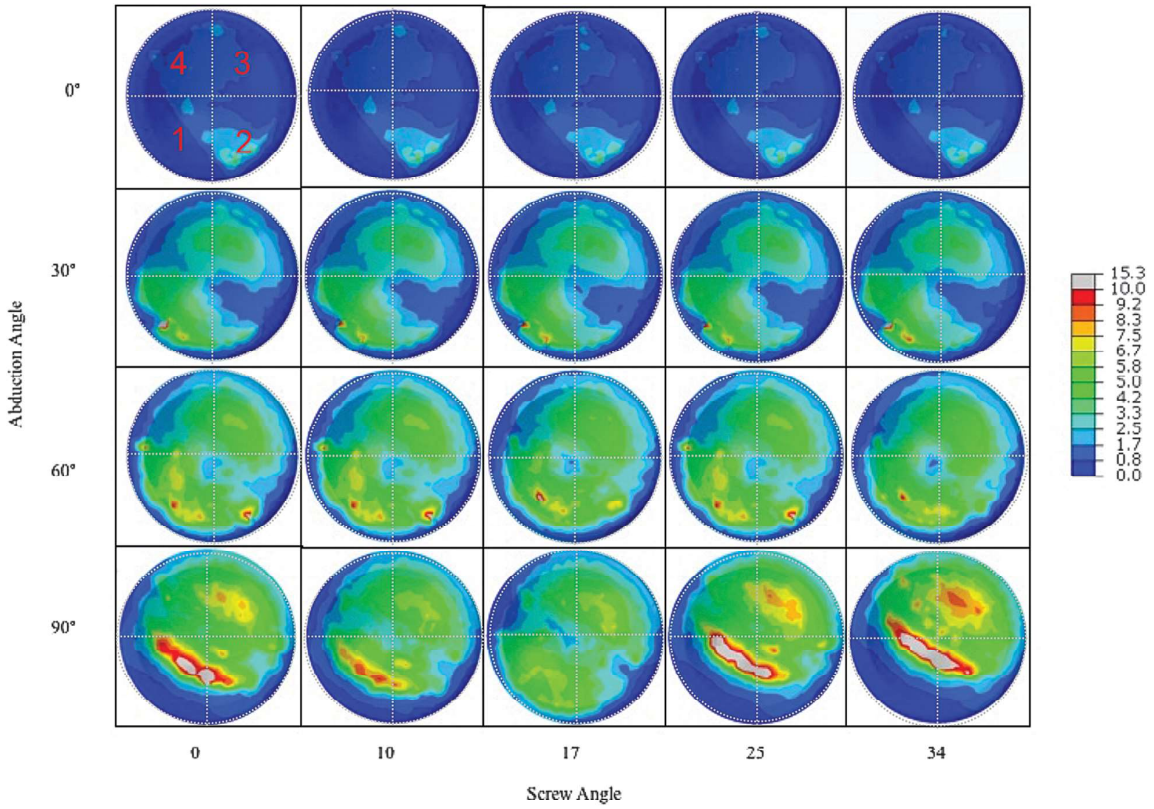

Fig. 8. The Von Mises stress distribution of humeral spacer.

and shoulder abduction occurred only on quadrant 3 and quadrant 4. However, this positive relationship was valid for quadrants 1, 2 up to 60 degrees of shoulder abduction. After that, the average contact stresses of quadrant 1 and 2 were decreased as the shoulder abduction angle reached 90 degrees.

Alternatively, if the shoulder abduction angle was fixed at 0 or 30 degrees, the average contact stresses in each quadrat remained almost constant as the screw angle increased (Fig. 7). However, for the higher abduction angles such as 60 degrees and especially 90 degrees, the average contact stresses on quadrants showed nonlinear behavior and the influence of SIA on quadrants became more clear (Fig. 7).

The most striking result was the distribution of contact stress on quadrants of the humeral spacer. According to the twenty stress distribution images that emerged from each analysis, there were significant differences between the 17 degree SIA cases and the others. The average contact stress due to the abduction of shoulder was more intense on quadrant 1 and 2 in all cases except the 17 degree SIA cases. Additionally, the most homogenous and the minimum stress distribution occurred when the SIA was 17 degrees (Fig. 8).

Overall, these results indicate that the average contact stress on the quadrants was influenced by variation of both the SIA and shoulder abduction angle.

4. DISCUSSION

The glenoid base plate fixation for reverse shoulder arthroplasty is a crucial step for improving long-term stability due to the excessive shear force transferred to the glenoid base plate by the deltoid leading to failure.[1,2,7,9,10,14,17,20,21,29–32] There has been no consensus about SIA and orientation due to the limited studies.[4,5,7,14,17,21,31] In this numerical study, we showed that the SIA used for the fixation of the glenoid base plate affected contact stress distribution on humeral spacer during the shoulder movements by employing the 20 different FE models.

The effect of SIA on the stress distribution of humeral spacer got more significant as the shoulder abduction reached 90 degrees where the maximum moment to the shoulder arm was applied. Another important finding at this position was about the stress concentration which may result in wear of the humeral spacer. The stress concentration occurred on the all angles except those of 17 degrees. All quadrants of the 17 degrees SIA had

less stress concentration and more homogeneous stress distribution in comparison to other SIA cases (Fig. 8).

In literature, there are studies which show the benefits of increasing the SIA on RSA.[17,20] Hopkins et al.[20] mentioned that the SIA increment played an important role on the glenoid baseplate since it reduced the interface micromotion between glenoid baseplate and bone. Moreover, Yang et al.[17] observed the similar FE results in their study in which the SIA diverged about 15 degrees. However, our study showed that a placement with a higher SIA is not always a favorable method for fixation of glenoid base plate at reverse shoulder arthroplasty and it might negative effects on other components of the implant system. This includes the humeral spacer which is most likely the first one to be affected by wear due to its rigidity. Therefore, the whole implant system should be taken into account since an interaction occurs between all the components. Since the screws are the bridging members from arm to shoulder, changing the SIA affects the transfer of the total load that is carried from arm to shoulder. It results in changing the load path direction of the arm in which each continuous load passes through neighboring members.

Haggard et al.[2] analyzed the effects of larger glenosphere diameters on the stability of RSA and humeral polyethylene wear. They concluded that the maximum stress could be observed in the inferior quadrant when smaller glenosphere diameters were used. Similar results were also obtained by Terrier et al.[30] They compared the anatomical shoulder prosthesis and reverse shoulder prosthesis in terms of polyethylene wear via FE model. They observed that contact stress on the polyethylene stayed on only the inferior and the edge region of the humeral spacer during the whole range of abduction.[30] Contrary to these studies, our results showed that the location of stress concentration generally occurred not only at the edge of quadrant 1, but also could be shifted to the central region of the quadrant with respect to the SIA. This could be seen in our findings for the cases of SIAs at 0, 10, 25, and 34 degrees, as the shoulder abduction reached higher angles such as 90 degrees. However, this phenomenon wasn't observed for the case of SIA at 17 degrees and more homogeneous stress distribution was obtained on all four quadrants at 90 degree of shoulder abduction (Fig. 8). Furthermore, the magnitude of the contact stress could also be changed regarding to the SIA. This phenomenon shows that the SIA affects not only the stress distribution but also the magnitude of the contact stress on humeral spacer due to the changes of direction of the transmitted load during the abduction.

It should be noted that the effects of the absence of different muscles can be neglected, since the study was performed in XY plane and also abduction is also in XY plane movement. Moreover, the variations of the SIA that were taken into account in this study cover only XY planes. The other planes should also be examined in a future study.

5. CONCLUSION

Glenoid complications have been related to multi-axial compressive force as well as compressive stress across the glenoid bone-baseplate interface which is provided by the humeral spacer. In order to maintain a long-term attachment between the baseplate and the glenoid bone, different baseplate fixation techniques have been used. The SIA placement is one of the important variables for base plate fixation. A stable interface is also related to regulate the stress distribution on all the components. This study describes a biomechanical approach to analyze stress distribution of the humeral spacer in reverse shoulder design regarding the different SIA placement of the baseplate in the absence of supraspinatus muscle status using a combination of *in vitro* mechanical analysis and finite element method. Shoulder abduction is not the only contributing parameter with regard to the average contact stress distribution on the quadrants, but the SIA also plays a major role on in this respect. It was also determined that a SIA placement at 17 degrees provided the optimal stress distribution on the humeral spacer. The effects of the absence of different muscles should also be examined in a future study.

Acknowledgments: We would like to thank Professor *MD*, Mehmet Demirtaş, Barış Sokollu, Emre Çelik, Nihat Özten, M. Barış Kösalı, Canberk Çıbık, Hannah van Rooyen, Alexander DiPaola and Saskia Hilbert-Kırkayak for their valuable contributions and support. We would like to also thank the Istanbul Technical University Research Foundation (İTÜ-BAP).

References and Notes

1. K. A. Lewicki, J. E. Bell, and D. W. Van Citters, Analysis of polyethylene wear of reverse shoulder components: A validated technique and initial clinical results. *J. Orthop. Res.* 35, 980 (**2017**).
2. J. Haggart, M. D. Newton, S. Hartner, A. Ho, K. C. Baker, M. D. Kurdziel, and J. M. Wiater, Neer Award 2017: Wear rates of 32-mm and 40-mm glenospheres in a reverse total shoulder arthroplasty wear simulation model. *J. Shoulder Elbow Surg.* 26, 2029 (**2017**).
3. C. Riley, J. Idoine, Y. Shishani, R. Gobezie, and B. Edwards, Early outcomes following metal-on-metal reverse total shoulder arthroplasty in patients younger than 50 years. *Orthopedics* 39, e957 (**2016**).
4. G. D. Langohr, R. Willing, J. B. Medley, G. S. Athwal, and J. A. Johnson, Contact mechanics of reverse total shoulder arthroplasty during abduction: The effect of neck-shaft angle, humeral cup depth, and glenosphere diameter. *J. Shoulder Elbow Surg.* 25, 589 (**2016**).
5. J. G. DiStefano, A. Y. Park, T. Q. Nguyen, G. Diederichs, J. M. Buckley, and W. H. Montgomery, 3rd, Optimal screw placement for base plate fixation in reverse total shoulder arthroplasty. *J. Shoulder Elbow Surg.* 20, 467 (**2011**).
6. O. Verborgt, A. I. Hachem, K. Eid, K. Vuylsteke, M. Ferrand, and P. Hardy, Accuracy of patient-specific guided implantation of the glenoid component in reversed shoulder arthroplasty. *Orthop. Traumatol. Surg. Res.* 104, 767 (**2018**).
7. B. F. Stephens, C. T. Hebert, F. M. Azar, W. M. Mihalko, and T. W. Throckmorton, Optimal baseplate rotational alignment for

locking-screw fixation in reverse total shoulder arthroplasty: A three-dimensional computer-aided design study. *J. Shoulder Elbow Surg.* 24, 1367 **(2015)**.

8. S. Carpenter, D. Pinkas, M. D. Newton, M. D. Kurdziel, K. C. Baker, and J. M. Wiater, Wear rates of retentive versus nonretentive reverse total shoulder arthroplasty liners in an *in vitro* wear simulation. *J. Shoulder Elbow Surg.* 24, 1372 **(2015)**.

9. J. S. Day, D. W. MacDonald, M. Olsen, C. Getz, G. R. Williams, and S. M. Kurtz, Polyethylene wear in retrieved reverse total shoulder components. *J. Shoulder Elbow Surg.* 21, 667 **(2012)**.

10. S. L. Smith, B. L. Li, A. Buniya, S. H. Lin, S. C. Scholes, G. Johnson, and T. J. Joyce, *In vitro* wear testing of a contemporary design of reverse shoulder prosthesis. *J. Biomech.* 48, 3072 **(2015)**.

11. N. S. Ribeiro, J. Folgado, P. R. Fernandes, and J. Monteiro, Wear analysis in anatomical and reversed shoulder prostheses. *Comput. Methods Biomech. Biomed. Engin.* 14, 883 **(2011)**.

12. D. Nam, C. K. Kepler, S. J. Nho, E. V. Craig, R. F. Warren, and T. M. Wright, Observations on retrieved humeral polyethylene components from reverse total shoulder arthroplasty. *J. Shoulder Elbow Surg.* 19, 1003 **(2010)**.

13. Z. Dai, P. Lei, Y. S. Zhang, H. Liu, W. Niu, K. Li, L. Wang, J. Xie, and Y. Hu, Effect of stimulation by ultrahigh molecular weight polyethylene wear particles on the osteogenesis capability of fibroblasts. *J. Biomater. Tissue Eng.* 8, 723 **(2018)**.

14. B. O. Parsons, K. I. Gruson, K. J. Accousti, R. A. Klug, and E. L. Flatow, Optimal rotation and screw positioning for initial glenosphere baseplate fixation in reverse shoulder arthroplasty. *J. Shoulder Elbow Surg.* 18, 886 **(2009)**.

15. L. Nalbone, R. Adelfio, M. D'Arienzo, T. Ingrassia, V. Nigrelli, F. Zabbara, P. Paladini, F. Campi, A. Pellegrini, and G. Porcellini, Optimal positioning of the humeral component in the reverse shoulder prosthesis. *Musculoskelet. Surg.* 98, 135 **(2014)**.

16. S. W. Chae, H. Lee, S. M. Kim, J. Lee, S. H. Han, and S. Y. Kim, Primary stability of inferior tilt fixation of the glenoid component in reverse total shoulder arthroplasty: A finite element study. *J. Orthop. Res.* 34, 1061 **(2016)**.

17. C. C. Yang, C. L. Lu, C. H. Wu, J. J. Wu, T. L. Huang, R. Chen, and M. K. Yeh, Stress analysis of glenoid component in design of reverse shoulder prosthesis using finite element method. *J. Shoulder Elbow Surg.* 22, 932 **(2013)**.

18. J. D. Webb, S. S. Blemker, and S. L. Delp, 3D finite element models of shoulder muscles for computing lines of actions and moment arms. *Comput. Methods Biomech. Biomed. Engin.* 17, 829 **(2014)**.

19. D. C. Ackland, S. Roshan-Zamir, M. Richardson, and M. G. Pandy, Muscle and joint-contact loading at the glenohumeral joint after reverse total shoulder arthroplasty. *J. Orthop. Res.* 29, 1850 **(2011)**.

20. A. R. Hopkins, U. N. Hansen, A. M. Bull, R. Emery, and A. A. Amis, Fixation of the reversed shoulder prosthesis. *J. Shoulder Elbow Surg.* 17, 974 **(2008)**.

21. C. S. Humphrey, J. D. Kelly, 2nd, and T. R. Norris, Optimizing glenosphere position and fixation in reverse shoulder arthroplasty, part two: The three-column concept. *J. Shoulder Elbow Surg.* 17, 595 **(2008)**.

22. C. J. Hung, C. L. Hsieh, P. L. Yang, and J. J. Lin, Relationships between posterior shoulder muscle stiffness and rotation in patients with stiff shoulder. *J. Rehabil. Med.* 42, 216 **(2010)**.

23. E. M. Brach Del Prever, A. Bistolfi, P. Bracco, and L. Costa, UHMWPE for arthroplasty: Past or future? *J. Orthop. Traumatol.* 10, 1 **(2009)**.

24. C. Oldani and A. Dominguez, Recent Advances in Arthroplasty, edited by D. S. Fokter, InTech., Rijeka **(2012)**.

25. H. Hermawan, D. Ramdan, and J. Djuansjah, Biomedical Engineering—From Theory to Applications, edited by R. Fazel-Rezai, Intech., Rijeka **(2011)**, Chap. 17, p. 411.

26. J. Rho, R. Ashman, and C. Turner, Young's modulus of trabecular and cortical bone material: Ultrasonic and microtensile measurements. *J. Biomech.* 26, 111 **(1993)**.

27. P. Buchler and A. Farron, Benefits of an anatomical reconstruction of the humeral head during shoulder arthroplasty: A finite element analysis. *Clin. Biomech. (Bristol, Avon)* 19, 16 **(2004)**.

28. A. Terrier, A. Reist, F. Merlini, and A. Farron, Simulated joint and muscle forces in reversed and anatomic shoulder prostheses. *J. Bone Joint Surg. Br.* 90, 751 **(2008)**.

29. J. M. Wiater and M. H. Fabing, Shoulder arthroplasty: Prosthetic options and indications. *J. Am. Acad. Orthop. Surg.* 17, 415 **(2009)**.

30. A. Terrier, F. Merlini, D. P. Pioletti, and A. Farron, Comparison of polyethylene wear in anatomical and reversed shoulder prostheses. *J. Bone Joint Surg. Br.* 91, 977 **(2009)**.

31. M. Harman, M. Frankle, M. Vasey, and S. Banks, Initial glenoid component fixation in "reverse" total shoulder arthroplasty: A biomechanical evaluation. *J. Shoulder Elbow Surg.* 14, 162S **(2005)**.

32. P. Boileau, D. J. Watkinson, A. M. Hatzidakis, and F. Balg, Grammont reverse prosthesis: Design, rationale, and biomechanics. *J. Shoulder Elbow Surg.* 14, 147S **(2005)**.

33. A. E. Bowden and J. Bergström, UHMWPE Biomaterials Handbook, edited by S. M. Kurtz, Third edn., William Andrew Publishing, Oxford **(2016)**, p. 753.

Received: 9 October 2018. Accepted: 26 October 2018.

RESEARCH ARTICLE